Optimizing Low-Frequency Mode Stirring Performance Using Principal Component Analysis

Luk R. Arnaut

***Abstract*—We formulate and perform principal component analysis (PCA) of mechanically stirred fields, based on tuner sweep data collected across a frequency band at a single location of a sensor inside a reverberation chamber. Both covariance- and correlation-based PCA in undermoded and overmoded regime are performed and intercompared. The nonstationarity of the stir performance as a function of the angular position of the stirrer is demonstrated. It is shown that this nonuniformity can be quantified and exploited to select a set of optimal stir angles. The rotated principal components are found to be interpretable as energy stirred by specific angular sectors of the stirrer and are related to the correlation structure of the data. The analysis leads to the concept of *eigenstirrings* (stir modes), which form an orthonormal set of empirical basis functions for expanding stir data.**

***Index Terms*—Multi-variate analysis, optimization, principal component analysis, reverberation chamber, statistical modelling.**

I. Introduction

STATIONARITY—also known as homogeneity—is a powerful concept in the theory of stochastic processes, particularly wide-sense stationarity (WSS). For analysis of fields in mode-tuned or mode-stirred reverberation chambers (MT/MSRCs), it allows for considerable simplification and progress in their statistical modeling [1], [2]. In essence, a random field is WSS if its first- and second-order statistics (in particular, its probability density function (PDF)/characteristic function, and its autocorrelation function (ACF)/power spectral density function, respectively) are independent of the choice of origins of space and time. As a result, first-order statistics of a WSS field such as its average, standard deviation, percentiles, etc., are statistically homogeneous in space and time, whereas the second-order properties, e.g., correlation length, coherence bandwidth, etc., depend only on the *difference* between space-time coordinates. Quantities that depend on both first- and second-order properties only (e.g., statistics of the extreme value of a Gaussian random field) are then also homogeneous. Mixed states are possible, e.g., a random field may be spatially homogeneous but temporally inhomogeneous, etc.

WSS is often prescribed as a prerequisite for statistical modeling of MT/MSRCs in an ideal setting [1], [3]. However, deviations from WSS are known to exist. For example, in the spatial domain, random fields and energy near an EM boundary exhibit different PDFs and ACFs compared to locations "deep" inside the cavity [4], [5]. In the time domain, nonstationarity is observed when a "time boundary" exist. For example, a pulse-modulated excitation yields time-variant distributions and correlations during the rise and decay in the received pulse response, in both mode-tuned [6] and mode-stirred [7] operation, or during step transitions [8]. In the stir domain (i.e., in sampled ensembles of statistically equivalent fields), WSS has so far been the default working assumption [9]. For an MT/MSRC exhibiting N uncorrelated field states at a fixed single frequency and location, one typically assigns N *uniformly separated* stir states, e.g., equal angular steps of a paddle wheel in mechanical stirring, frequency steps in frequency stirring, separated locations in source stirring, etc. However, glimpses of nonstationarity in the stir domain (i.e., nonuniform stir performance across uniformly sampled stir states) have previously been observed. For example, at relatively low frequencies, sudden irregular jumps were detected in the steady-state energy levels (cf., the interval $650\,\mathrm{s} < t < 750\,\mathrm{s}$ in [8, see Fig. 2(a)]). At higher frequencies, such jumps are harder to detect, because they are masked by the increased fluctuation (variance) of the stir process. Nevertheless, indirectly, the nonuniform increase of N with frequency, especially the occurrence of intermediate plateaus of stir performance $N(f)$ where such increase stalls, has been observed even at gigahertz frequencies [10, Fig. 10], [11, Figs. 2, 3, 12]. Specifically, in [11, Fig. 12], the plateau disappears when the number of sampled stir states is approximately quadrupled at constant stir speed. This suggests that certain better performing stir states can easily be missed if the sampling rate is too low.

In this paper, we apply principal component analysis (PCA) [12]–[15] to evaluate the stir performance of individual stir states across a specified frequency interval, thus abandoning the assumption of WSS. In the context of MT/MSRCs, functional PCA (also known as orthogonal expansion) was already introduced in [17, Section IV.2], [18], to eliminate arbitrariness in the choice of correlation threshold level to estimate N. Here, the emphasis is on (but not limited to) operation at relatively low frequencies, aiming to further reduce the lowest usable frequency (LUF) by identifying superior stir states. Thus, rather than being an undesirable property, nonstationarity offers scope for achieving a better-than-average stir performance. Although the performance may become frequency- and location-specific, PCA can optimize these frequencies and locations as well, by using a dual formulation. Without loss of generality, we consider mechanical stirring through angular rotation of a single paddle wheel. The field is received at a single spatial location

Manuscript received February 18, 2013; revised April 26, 2013; accepted June 5, 2013. Date of publication July 31, 2013; date of current version January 27, 2014.

The author is with the George Green Institute of Electromagnetics Research, University of Nottingham, University Park, Nottingham NG7 2RD, U.K. (e-mail: luk.arnaut@nottingham.ac.uk).

Color versions of one or more of the figures in this paper are available online at http://ieeexplore.ieee.org.

Digital Object Identifier 10.1109/TEMC.2013.2271903

and orientation of the sensor, measured across a frequency interval. The formalism is confined here to real-valued fields, but extends effortlessly to circular complex fields.

Overbar ($\overline{X}$) and bracket ($\langle X \rangle$) notations refer to sample and ensemble averagings, while Roman uppercase and corresponding lowercase symbols denote random variables and their values, respectively, except for matrix dimensions and their indices. Nil, single, and double underlined quantities represent scalars, vectors, and matrices, respectively.

II. Basic Concepts

A. Motivation

In the context of MT/MSRCs, PCA identifies a specific set of N states based on a larger set of M original correlated stir states, such that the combined stirred energy produced by these fewer states is close to the total stirred energy for all M states. Here, "close" means substantially higher than the average fraction N/M expected if the N states were selected by simple random sampling. The N states cannot be truly "equivalent" to the original M, because all stirred energy can be fully captured only if $N = M$. However, if the correlation between the M states is strong, then a subset of N states may yield negligible loss of stir performance.

Unlike classical decimation based on uniform sampling at regular intervals starting at an arbitrary stir state, PCA identifies groups of weighted stir states that are ranked according to the maximum residual stirred energy, as will be shown.

B. PCA Algorithm

The general method of PCA is described extensively in the literature, e.g., [12]–[14]. Here, we formulate the technique in terms of its application to MT/MSRCs. The correlation structure of the stir states is either assumed to be known *a priori* or can be estimated from a set of observations. PCA calculates specific *linear* combinations of stir states, called principal components (PCs), based on the observed (measured) values of the stirred field. The expansion (weight) coefficients for the stir states in each PC are chosen iteratively, such that:

1) the first PC captures the maximum fraction of the stirred energy (variance) in the dataset of stir sequences;
2) each subsequent (nth) PC:
   a) maximizes the remainder stirred energy (residual variance), after the contributions by the $n-1$ previous PCs have been removed;
   b) accounts for a fraction of the stirred energy that does not exceed any of the $n-1$ previous fractions;
   c) is chosen to be uncorrelated with, and having a direction orthogonal to all $n-1$ previous PCs (orthogonal PC loadings and uncorrelated PC scores).

The optimal weights of the PCs are obtained by minimizing the distance of the original data to their best fitting hyperplane (subspace) [12]. This is achieved by ranking and truncating the PCs according to the contributing variance (stirred energy) of each PC. PCA not only identifies the best stir states, but also provides patterns of linear relationships between them. Other uses of PCA (e.g., outlier detection) are not addressed here.

As with any correlation based analysis, PCA only yields components that are *linearly* independent. If the random data are not Gaussian, then the extracted PCs may still exhibit higher order correlations. However, the applicability of PCA does not depend at all on the PDF of the data.

C. Terminology and Notations

Based on standard terminology in PCA, when the goal is to analyze stir performance, each (mth) stir state τ_m represents a *variable*, with $m = 1, \ldots, M$. The field X measured at one of P independent[1] values of a chosen parameter o_p for the field sensor (i.e., its location/orientation/measurement frequency/etc.) across all M stir states is the pth *observation* (or *sample*) of X, with $p = 1, \ldots, P$. It is represented by a single continuous *stir trace* function $x_p(\tau)$ in MSRCs, or by a $1 \times M$ row vector *stir sequence* $\underline{x}_p^T = [x_{p1}, \ldots, x_{pM}]$ in MTRCs or sampled MSRCs. For example, if sensor locations constitute the observations, then each observation is obtained at an arbitrary location for a fixed sensor orientation, measurement frequency, etc.; by contrast, if frequency is chosen as the observation quantity, then each observation is a stir sequence/trace at an arbitrary frequency, for a fixed sensor orientation, location, etc. The M stir states sampled across the observations form a $P \times M$ *data matrix* $\underline{\underline{x}} \equiv [\underline{x}_m] \equiv [x_{pm}]$ with columns $\underline{x}_m$ of size $P \times 1$, containing all observations of the field for the mth stir state. This matrix is either mean-centered to $\underline{\underline{y}} \equiv [\underline{y}_m] = [\underline{x}_m - \overline{\underline{x}_m}]$ in covariance-based PCA, or standardized to $\underline{\underline{z}} \equiv [\underline{z}_m] \equiv [(\underline{x}_m - \overline{\underline{x}_m})/s_{\underline{x}_m}]$ in correlation-based PCA. The sample average $\overline{\underline{x}_m}$ and standard deviation $s_{\underline{x}_m}$ are taken across all P observations in the mth column.

Based on $\underline{\underline{y}}$ or $\underline{\underline{z}}$, PCA builds an $M \times N$ *loading* or *component matrix* $\underline{\underline{a}} \equiv [\underline{a}_n] \equiv [a_{mn}]$. On application of the PCA algorithm described in Section II-B, the loading vectors $\underline{a}_n$ of $\underline{\underline{a}}$ are found to be (re-)normalized $M \times 1$ column eigenvectors (EVEs) $\underline{\psi}_n$ of the $M \times M$ sample autocovariance matrix $\underline{\underline{c}} \triangleq \overline{\underline{\underline{y}}^T \cdot \underline{\underline{y}}}/P$ or autocorrelation matrix (ACM) $\underline{\underline{k}} \triangleq \overline{\underline{\underline{z}}^T \cdot \underline{\underline{z}}}/P$, with associated eigenvalues (EVAs) λ_n^2. Each *loading (coefficient)* a_{mn} is the expansion coefficient (projection coordinate) for the mth state of the stirred field $\underline{y}_m$ or $\underline{z}_m$ with respect to the nth principal direction $\underline{1}_n = \underline{\psi}_n / \|\underline{\psi}_n\| = \underline{a}_n / \|\underline{a}_n\|$, i.e., it measures the similarity (correlation) between the mth stir state and the nth PC. For a random stir sequence $\underline{Z}^T$, the nth ensemble PC is then specified by

$$S_n \triangleq \underline{Z}^T \cdot \underline{a}_n = \sum_{m=1}^{M} Z_m a_{mn}, \quad n = 1, \ldots, N, \ldots, M. \quad (1)$$

The PCA algorithm extracts a subset of N PCs with scores $s_n \triangleq \underline{z}^T \cdot \underline{a}_n = \sum_{m=1}^{M} z_m a_{mn}$ in N iterations and terminates

[1] The requirement for all P observations of X to yield statistically independent field values is only necessary when *distributions* of eigenvalues and principal components are of interest. PCA also applies to correlated observations, without loss of validity [15], provided that $P \gg 1$, i.e., a sufficiently large sample in order to be representative of the ensemble.

according to a chosen selection criterion, yielding a $1 \times N$ sample PC vector $\underline{s}^T = [s_n]$. Note that for an assumed known correlation structure of the field, the $\underline{a}_n$ in (1) are deterministic, not random vectors even for random fields. If, however, the ACM for $\underline{Z}^T$ needs to be estimated from $\underline{z}^T$, then the $\underline{a}_n$ become samples of random loading vectors $\underline{A}_n$.

The *score* of the pth specific *observed* stir sequence $\underline{z}_p^T$ with respect to the nth sample PC is $s_{pn} \triangleq \underline{z}_p^T \cdot \underline{a}_n = \sum_{m=1}^M z_{pm} a_{mn}$, i.e., the projection of $\underline{z}_p^T$ onto the nth eigendirection, yielding the coordinate of this observation field vector with respect to the nth principal axis. The s_{pn} have the same physical unit as z. They combine to a $P \times N$ *score matrix*

$$\underline{\underline{s}} = \underline{\underline{z}} \cdot \underline{\underline{a}}. \tag{2}$$

The score vector for any new observation $\underline{z}_{p'}^T$ at a frequency $f_{p'}$ is then $\underline{s}_{p'}^T = \underline{z}_{p'}^T \cdot \underline{\underline{a}}$. The *leverage* of the scores, $\underline{h} \triangleq \underline{s} \cdot (\underline{\underline{s}}^T \cdot \underline{\underline{s}})^{-1} \cdot \underline{\underline{s}}^T$, measures the rotating power of the data about their center, indicating how well the extracted PCs model the data.

In standard normalization of PCs, $\underline{a}_n^T \cdot \underline{a}_n \equiv \sum_{m=1}^M a_{mn}^2 \triangleq 1$, i.e., the a_{mn} are the direction cosines of a stir sequence $\underline{z}^T$ relative to the nth principal axis along $\underline{1}_n$. With this normalization, the a_{mn} are related to the product-moment correlation coefficients between $\underline{Z}^T$ and $\underline{S}$, i.e., to

$$\rho_{mn} \triangleq \frac{\langle (Z_m - \langle Z_m \rangle)(S_n - \langle S_n \rangle) \rangle}{\sqrt{(Z_m - \langle Z_m \rangle)^2}\sqrt{(S_n - \langle S_n \rangle)^2}} \tag{3}$$

by the expression $a_{mn} = \rho_{mn}/\sqrt{\lambda_n^2}$, or their sample equivalents. Instead, if $\underline{a}_n^T \cdot \underline{a}_n \triangleq \lambda_n^2$ is chosen as normalization, then $a_{mn} = \rho_{mn}$ [13], so that the summed squared PC loadings across all M stir states then yield the nth EVA as

$$\lambda_n^2 = \sum_{m=1}^M a_{mn}^2 = \sum_{m=1}^M \rho_{mn}^2, \quad n = 1, \ldots, N \tag{4}$$

with $\sum_{n=1}^M \lambda_n^2 = M$. The proportion of the total stirred energy (i.e., variance of the stirred field) explained by the nth PC is

$$\eta_n^2 = \frac{\lambda_n^2}{\sum_{m=1}^M \lambda_m^2}, \quad n = 1, \ldots, N, \ldots, M. \tag{5}$$

Instead, if reference is made to the *extracted* variance for N PCs, then M in (5) must be replaced by N.

Another useful concept is the *communality* $\kappa_N(m)$ of $\underline{z}_m$, representing the proportion of the stirred energy accounted for by the mth stir state $\underline{z}_m$ that it shares (has in common with, contributes to) the energy extracted by the first N PCs. For $\underline{a}_n^T \cdot \underline{a}_n \triangleq \lambda_n^2$, this is the sum of N energy *contributions* a_{mn}^2 of a particular $\underline{z}_m$ across the columns of $\underline{\underline{a}}$, i.e.,

$$\kappa_N(m) = \sum_{n=1}^N a_{mn}^2 = \sum_{n=1}^N \rho_{mn}^2 \leq 1, \quad m = 1, \ldots, M \tag{6}$$

because the proportion of variance explained by a regression model and statistical effect size are generally expressed by the coefficient of (partial) determination ρ_{mn}^2. Naturally, $\kappa_{N=M}(m) = 1$ and $\sum_{m=1}^M \kappa_M(m) = M = \sum_{n=1}^M \lambda_n^2$. When using standard normalization, $\kappa_N(m) = \sum_{n=1}^N a_{mn}^2 \lambda_n^2$.

TABLE I
STIR SEQUENCES, LOADINGS, PCS, SCORES, EIGENVALUES AND COMMUNALITIES FOR CORRELATION-BASED PCA

$\cdot$	$\underline{a}_1$	$\underline{a}_2$	$\ldots$	$\underline{a}_N$
$\underline{z}_1^T$	s_{11}	s_{12}	$\ldots$	s_{1N}
$\underline{z}_2^T$	s_{21}	s_{22}	$\ldots$	s_{2N}
$\vdots$	$\vdots$	$\vdots$	$\vdots$	$\vdots$
$\underline{z}_P^T$	s_{P1}	s_{P2}	$\ldots$	s_{PN}
$\underline{Z}^T$	S_1	S_2	$\ldots$	S_N
for $\underline{a}_n^T \cdot \underline{a}_n = \lambda_n^2$:				
$\sum_{m=1}^M a_{mn}^2$	λ_1^2	λ_2^2	$\ldots$	λ_N^2
$\sum_{n=1}^N a_{mn}^2$	κ_1	κ_2	$\ldots$	κ_N
for $\underline{a}_n^T \cdot \underline{a}_n = 1$:				
var$(\underline{Z}^T \cdot \underline{a}_n)$	λ_1^2	λ_2^2	$\ldots$	λ_N^2
$\sum_{n=1}^N a_{mn}^2 \lambda_n^2$	κ_1	κ_2	$\ldots$	κ_N

Similar to good practice in linear regression analysis, when extracting N PCs one typically requires $P \geq 2N, \ldots, 5N$, as a rule-of-thumb, in order to get sufficient accuracy in estimating the sample EVEs and EVAs (and, hence, PCs), because the variance on the nth score is λ_n^2/P.

In the remainder, we shall generalize all sampled quantities to random (ensemble) quantities.

III. PRE-PCA OPERATIONS AND CONSIDERATIONS

A. Inspection of Correlation Matrix

Before embarking on a PCA, it is advisable to check whether selecting stir states may offer any gains at all, i.e., whether there is sufficient inhomogeneity in the stirred energy to offer a prospect of extracting optimum states. To this end, we inspect the sample $\underline{k}$ of the the 2-D symmetric ACM $\underline{\underline{K}} \equiv [\varrho_{mn}]$, where

$$\begin{aligned} \varrho_{mn} &\equiv \varrho_X(\tau_m, \tau_n) = \langle (\underline{Z}_m - \langle \underline{Z}_m \rangle)^T \cdot (\underline{Z}_n - \langle \underline{Z}_n \rangle) \rangle \\ &\triangleq \frac{\langle (\underline{X}_m - \langle \underline{X}_m \rangle)^T \cdot (\underline{X}_n - \langle \underline{X}_n \rangle) \rangle}{\sqrt{(\underline{X}_m - \langle \underline{X}_m \rangle)^2}\sqrt{(\underline{X}_n - \langle \underline{X}_n \rangle)^2}} \end{aligned} \tag{7}$$

where the samples of the field X at observation points o_p for the mth stir state τ_m are contained in the vector

$$\underline{X}_m \triangleq [X(o_1; \tau_m), \ldots, X(o_P; \tau_m)]. \tag{8}$$

This 2-D generalization of the 1-D ACF vector (correlogram) $[\varrho_X(\tau_m - \tau_n)]$ for WSS stir sequences is obtained by taking each τ_n in turn as a reference state, against which the two-point correlation coefficient with all other τ_m is calculated. A WSS stir process produces a Töplitz circulant ACM with banded structure [17], [18]. Any deviation from this structure indicates stir inhomogeneity. Here, our interest is in those zones within $\underline{\underline{K}}$, where ϱ_{mn} is close to zero, indicating sets of pairs of uncorrelated stir states (cf., Section VI). A row or column in $\underline{\underline{K}}$ that has $|\varrho_{mn}| \simeq 0$ throughout (except on the main diagonal, where $\varrho_{mn} = 1$) corresponds to single stir state that is itself a PC. While this is attractive with a view to maximize N, it does not necessarily maximize the total stirred energy.

In principle, the targeted optimum stir states could also be guessed from inspection of $\underline{\underline{K}}$. However, this method is subjective and becomes difficult to apply beyond the first two dominant stir states. As will be shown, it can even be misleading in some cases. This is because the ϱ_{mn} are standardized quantities, which do not permit deciding which one of two pairs of candidate states maximizes the combined stir performance. For example, a stir state τ_n may be strongly uncorrelated to two mutually strongly correlated states τ_{m_1} and τ_{m_2}, yielding $|\varrho_{m_1 n}|, |\varrho_{m_2 n}| \sim 0$, but perhaps with a high value of $\varrho_{m_1 m_2} \equiv s_{XX}(m_1, m_2)/[s_X(m_1)s_X(m_2)] \sim 1$. However, the value of $\varrho_{m_1 m_2}$ itself does not give information about the relative stir performance at m_1 versus m_2, i.e., the magnitude of $s_X(m_1)/s_X(m_2)$. Instead, PCA offers an objective and systematic technique for ranking (clusters of) stir states and their contributions to the total stirred energy. Pairs of strongly uncorrelated stir states in the ACM ($|\varrho_{mn}| \sim 0$) suggest *candidate* PCs; their actual contribution to the stirred energy follows in conjunction with the EVAs.

B. Selection Criterion for Number of PCs to be Extracted

A major issue in PCA is deciding on the number of PCs N to be retained, and the justification of any threshold value (or other metric) defining this number. This bears resemblance to the similar issue of finding "the" number of "equivalent" independent stir states from analysis of the ACF for WSS stirring [10], [19]–[25]. In addition to its obvious effect on the accuracy of representing the actual stir data by accounting for a large but incomplete fraction of the stirred energy, the choice of N also has an effect on the rotation and physical interpretation of PCs (cf., Section V-B). Several *ad hoc* rules exist [14], [26], which are briefly summarized and evaluated here for use with MT/MSRC data.

Cattell's rule selects N at or below the first point of inflexion in the "scree" plot of high-to-low ranked EVAs versus PC number. For MT/MSRCs, this rule appears to be inapplicable because in our analysis, the piecewise sequence of EVAs always decreases with with a positive (convex) curvature throughout.

The Guttman–Kaiser criterion [27] retains only those PCs whose EVAs λ_n^2 are larger than 1. The rationale is that such PCs contain more than the average variance (stirred energy) shared among all M variables. Each EVA represents how many times the equivalent average stirred energy is comprised in the PC associated with this EVA. Here, the fictitious "equivalent average" stirred energy is what would be obtained if all the stirred energy were equally shared by all M states (WSS process). Thus, the Guttman–Kaiser criterion suggests to retain only those PCs that are *comparatively* more significant than the others with $\lambda_n^2 < 1$. However, since there could be many small EVAs that together form a substantial fraction of the total stirred energy, this criterion typically underestimates N. Sometimes the threshold value 1 is lowered *ad hoc* to 0.7 [15]. For MT/MSRC data, which are characterized by long-tailed (slowly decaying) EVA sequences, this lowering increases the number of retained PCs substantially. Nevertheless, discarding the $M - N$ remainder PCs with EVA below 1 can still result in a significant shortfall in the stirred energy accounted for by the N retained states. A significance test for absolute contributions is Bartlett's test for the smallest $V = M - N$ EVAs to be zero, with the $\chi^2_{\frac{1}{2}(V-1)(V-2)}$ test statistic

$$\nu \left[V \ln \left(\frac{\sum_{k=N+1}^{M} \lambda_k^2}{V} \right) - \sum_{k=N+1}^{M} \ln \left(\lambda_k^2 \right) \right] \tag{9}$$

where ν is the number of degrees of freedom (rank of $\underline{\underline{K}}$).

From a different perspective, one could envisage the N PCs as "signals" and the remainder $M - N$ components as "noise," where the latter produce fluctuating stir performance but add no mean stirred energy. A result from information theory for blind source separation in a multichannel time series then states that the minimum code descriptor length (MDL) of the data [28], [29] provides an objective estimation of N as the value that minimizes the function

$$\mathrm{MDL}(N) = -(M-N)P \ln \left[\frac{\prod_{i=N+1}^{M} (\lambda_i^2)^{1/(M-N)}}{\sum_{i=N+1}^{N} \lambda_i^2/(M-N)} \right] + \frac{(2M-N)N}{2} \ln(P). \tag{10}$$

For $P \to \infty$, this metric yields consistent estimates of N, unlike Akaike's information criterion (AIC) [29]. Generally, MDL and AIC estimates of N are found to be considerably lower than those obtained by the aforementioned criteria.

Cross validation [30] is a more intensive resampling technique, in which one PC is eliminated at a time. Here, the distance of this component to the value estimated from a model based on $P - 1$ other components (predicted residual sum of squares (PRSS)) is minimized.

Another criterion selects N on the basis of a specified minimum proportion of cumulative variance $\sum_{n=1}^{N} \eta_n$ retained by the N largest EVAs, with recommended values typically ranging between 75% and 90% [15]. While a physical foundation for the selected confidence or significance level is lacking, it may produce more realistic values for N. An extension is the Wachter plot, which is a Q–Q plot of the sample EVAs versus quantiles of the Marčenko–Pastur semicircle limit density for the EVAs, a result based on random matrix theory and asymptotic PDFs of EVAs [31].

In summary, several comparisons of the predicted values of N for some of these rules and others [14], [15], [26] all indicate that no single rule is superior: their accuracy depends on the specific level of data correlation. In our experimental results, we will compare the Guttman–Kaiser and MDL-AIC criteria. Although important for the practical implementation, it is emphasized that the determination of N is a not the focus of PCA. Rather, PCA addresses a follow-on question, i.e., *given* a value of N, find the set of N variables that maximizes the stirred energy.

C. Covariance-Versus Correlation-Based PCA

In general, covariance- and correlation-matrix based PCA yield different PCs, because autocovariance and autocorrelation matrices have different eigendecompositions. Covariance-based PCs are generally more easily interpretable. However, the

decisive factor in choosing between both methods is the level of inhomogeneity of the variance (heteroscedasticity) of sequences of observations between stir states: covariance-based PCA requires near-homogeneity (quasi-homoscedasticity) in order to detect correlations between weaker stir states. In MT/MSRC applications, substantial heteroscedasticity is often found, e.g., in wideband operation and/or undermoded chambers for frequency as the observation quantity (as a result of strong frequency dispersion), or in statistically anisotropic vector fields near PEC walls for sensor location/orientation as the observations (due to polarization dispersion). Correlation-based PCA has several other advantages, including scale invariance [15]. Ultimately, however, both approaches maximize the variance of the *standardized* variables [15, p. 42]. This should be especially remembered when unstandardizing PCs in postprocessing (cf., Section V-C).

D. Choice of Observation Parameter

PCA requires generating data through multiple observations at each variable (stir state). To optimize stir performance in order to minimize the LUF, one is ideally interested in generating observations at a *single* frequency, e.g., by varying the location or orientation of the transmitting or receiving antenna. Choosing the sensor location $\underline{r}$ as the observation parameter $[(o_1,\ldots,o_P)\equiv(\underline{r}_1,\ldots,\underline{r}_P)]$ has several benefits compared to choosing the frequency f $[(o_1,\ldots,o_P)\equiv(f_1,\ldots,f_P)]$. First, the extracted optimum stir states at a single frequency are not affected by any frequency dispersion of the stir performance. Such dispersion may be particularly strong near the LUF, so that optimization based on observations across a narrow band may yield a different optimum than obtained for a wider band. Second, observations at different spatial locations yield optimum stir states that apply[2] across the 3-D volume spanned by these locations, e.g. at the corners of a cubic or other working volume [9] enclosing an EUT. On the other hand, this inherent dependence on different locations implies that the optimum stir states ignore statistical spatial inhomogeneity (spatial dispersion), which is stronger near the LUF than at higher frequencies. This issue is dual to the frequency dispersion associated with observation frequencies. In addition, the mechanics of sensor displacements for generating of different locations are more cumbersome and time consuming, compared to frequency scanning for generating frequency observations.

In practice, changes in the field caused by moving a probe or cabling layout between locations may limit the generality of the optimization result. Since existence of some data correlation between different observations is not a fundamental issue (cf., Section II-C), one may choose the spatial locations at relative distances that are slightly below the ideal spatial correlation length, i.e., between $\lambda/4$ and $\lambda/2$ (or in excess of $\lambda/2$ near conducting boundaries [16]), to maximize P and hence minimize uncertainty. One could also choose mixed frequency and spatial locations as observations (3-D PCA), analyzed with tensorial PCA techniques or by vectorizing the data and applying 2-D PCA.

[2]Strictly, the optimization applies only at the specifically chosen spatial locations. The optimum may be expected to extend to other points within the spanned volume if this volume is not electrically large in any dimension.

IV. PCA Computation

A. Orthogonal Expansion (Karhunen–Loève Expansion, Functional PCA)

In the context of EMC and MT/MSRCs, orthogonal expansion (OE) was introduced in [17], [18]. While closely related to PCA, it is typically used with continuous functions, i.e., unsampled stir traces. We show that solutions obtained by OE and PCA satisfy the same characteristic equation, i.e., both methods select the same stir states in the continuum limit. For large M and N, the eigenfunctions for OE are known in closed form [17], providing an efficient alternative to PCA.

Consider $Z(\tau)=[X(\tau)-\langle X(\tau)\rangle]/\sigma_{X(\tau)}$ at the continuum stir state τ, representing a stochastic stirred field (ensemble of random continuous stir trace functions). A sample function $z(\tau)$ is realized by selecting an arbitrary frequency/location/orientation of the sensor. The random stir trace $Z(\tau)$ can be expanded into a linear combination of N deterministic continuous basis functions $\psi_n(\tau)$ with random expansion coefficients Z_n as

$$Z(\tau)=\operatorname*{l.i.m.}_{N\to\infty}\sum_{n=1}^{N}Z_n\psi_n(\tau),\quad Z_n=\int_0^{\mathcal{T}}Z(\tau)\psi_n(\tau)\mathrm{d}\tau. \tag{11}$$

Generally, the $\psi_n(\tau)$ are arbitrary complex-valued functions. In OE, they are chosen to form a complete orthonormal set such that the random coefficients are uncorrelated, i.e.,

$$\langle(Z_n-\langle Z_n\rangle)(Z_m-\langle Z_m\rangle)^*\rangle=\lambda_n^2\delta_{nm}. \tag{12}$$

Substituting (11) into (12) leads to the condition

$$\int_0^{\mathcal{T}}\psi_n(\tau)\left[\int_0^{\mathcal{T}}K(\tau,\mu)\psi_m^*(\mu)\mathrm{d}\mu\right]\mathrm{d}\tau=\lambda_n^2\delta_{nm} \tag{13}$$

for all m and n, where $K(\tau,\mu)\triangleq\langle(Z(\tau)-\langle Z(\tau)\rangle)(Z(\mu)-\langle Z(\mu)\rangle)^*\rangle$ is the two-point ACF evaluated at (τ,μ). Nontrivial solutions of (13) require that

$$\int_0^{\mathcal{T}}K(\tau,\mu)\psi_n^*(\mu)\mathrm{d}\mu=\lambda_n^2\psi_n^*(\tau) \tag{14}$$

which is satisfied by the condition

$$K(\tau,\mu)-\lambda_n^2\delta(\tau-\mu)=0. \tag{15}$$

For stir traces sampled at $\tau_m=m\Delta\tau$, the stir trace function and basis functions are discretized to

$$X(\tau)=\sum_m X_m\tilde{\delta}(\tau-\tau_m),\quad \psi_n(\tau)=\sum_m\psi_{nm}\tilde{\delta}(\tau-\tau_m) \tag{16}$$

where $\tilde{\delta}(\cdot)$ is the discrete unit-amplitude sampling comb function. In vector format

$$\underline{X}=[X_m(\tau_m)]_{m=1}^M,\quad \underline{\psi}_n=[\psi_{nm}(\tau_m)]_{m=1}^M. \tag{17}$$

After standardizing $\underline{X}$ and applying point matching to (15), the uncorrelatedness of the sample coefficients (12) leads to

$$\left(\underline{\underline{K}}-\lambda_n^2\underline{\underline{I}}\right)\cdot\underline{\psi}_n=\underline{0} \tag{18}$$

for the $M \times M$ ACM $\underline{\underline{K}}(m,n)$, whose EVAs λ_n^2 are solutions of the characteristic equation

$$\det(\underline{\underline{K}} - \lambda_n^2 \underline{\underline{I}}) = 0. \tag{19}$$

If $\underline{\underline{K}}$ is Hermitean (WSS), then all λ_n^2 are positive and $\underline{\psi}_n$ are real. With (11), if $Z(\tau)$ is Gaussian then the Z_n are also Gaussian.

B. Variance Maximization

Equation (19) also corresponds to the solution of an iterative variance maximization problem for a random stir sequence $\underline{Z}$ as aimed for in PCA, as shown next.

In the first iteration, the vector $\underline{a}_1$ that maximizes $\mathrm{var}(\underline{Z}^T \cdot \underline{a}_1) \equiv \underline{a}_1^T \cdot \underline{\underline{K}} \cdot \underline{a}_1$, i.e., contains the maximum stirred energy subject to the constraint that $\underline{a}_1^T \cdot \underline{a}_1 = 1$, follows by the method of Lagrange multiplication as

$$\underline{a}_1^T \cdot \underline{\underline{K}} \cdot \underline{a}_1 - \lambda_1^2(\underline{a}_1^T \cdot \underline{a}_1 - 1) = 0. \tag{20}$$

The derivative of (20) with respect to $\underline{a}_1$ yields (19) for $n = 1$. Since $\langle \underline{Z} \rangle = 0$, this EVE also maximizes the mean square, i.e., $\langle (\underline{Z}^T \cdot \underline{a}_1)(\underline{Z}^T \cdot \underline{a}_1) \rangle = \underline{a}_1^T \cdot \underline{\underline{K}} \cdot \underline{a}_1 = \lambda_1^2 \underline{a}_1^T \cdot \underline{a}_1 = \lambda_1^2$. Thus, the EVE associated with the largest EVA $\lambda_1^2 = \mathrm{var}(\underline{Z}^T \cdot \underline{a}_1)$ extracts the maximum stirred energy λ_1^2. In successive iterations, with the subsequent conditions that $\mathrm{cov}(\underline{Z}^T \cdot \underline{a}_1, \underline{Z}^T \cdot \underline{a}_2) = \cdots = \mathrm{cov}(\underline{Z}^T \cdot \underline{a}_1, \underline{Z}^T \cdot \underline{a}_n) = \underline{0}$, it follows that conditional variance maximization yields

$$\lambda_n^2 = \mathrm{var}(\underline{Z}^T \cdot \underline{a}_n) \equiv \mathrm{var}(\underline{Z}^T \cdot \underline{\psi}_n) \tag{21}$$

as the maximum remainder (i.e., the thus far unaccounted) stirred energy extracted by $\underline{a}_n$ in the nth iteration, where $\lambda_n^2 \le \lambda_{n-1}^2 \le \cdots \le \lambda_1^2$. In other words, each EVE $\underline{\psi}_n$ accounts for $(100 \times \lambda_n^2/M)\%$ of the total stirred energy. Ranking the EVAs from high to low, the share of stirred energy decreases progressively.

Naturally, if all M PCs were extracted ($N = M$), then no information is lost, but no reduction is gained either. Nevertheless, ranking of all M contributions to the total stirred energy can still provide useful insight into the data structure.

C. Decomposition of Correlation and Field Matrices

In order to detect the structure of the ensemble ACM $\underline{\underline{K}} = \langle \underline{Z}\,\underline{Z}^T \rangle = \lim_{P\to\infty} \overline{\underline{Z}^T \cdot \underline{Z}}/P$ and to determine how different stir states might contribute to it, it is instructive to decompose $\underline{\underline{K}}$ in terms of its EVEs $\underline{\psi}_n$ as its natural axes. To this end, recall that the $M \times N$ component matrix $\underline{\underline{A}}_N$ used with the standard PC normalization is orthonormal, i.e., $\underline{\underline{A}}_N^T \cdot \underline{\underline{A}}_N = \underline{\underline{I}}_N$, where a subscript N denotes limitation to the first N rows and columns of $\underline{\underline{A}}$, with zeros replacing the last $M - N$ row and column entries. A singular value decomposition (SVD) of $\underline{\underline{Z}}$ yields

$$\underline{\underline{Z}}_N = \underline{\underline{U}}_N \cdot \underline{\underline{\Lambda}}_N \cdot \underline{\underline{A}}_N^T \tag{22}$$

where $\underline{\underline{\Lambda}}_N = (\underline{\underline{\Lambda}}_N^2)^{1/2} = \mathrm{diag}(\sqrt{\lambda_1^2}, \ldots, \sqrt{\lambda_N^2})$. The $P \times N$ matrix $\underline{\underline{U}}_N$ is orthonormal with nth column $\underline{U}_n \triangleq \underline{\underline{Z}}_N \cdot \underline{\psi}_n / \sqrt{\lambda_n^2}$, so that $\underline{\underline{U}}_N = \underline{\underline{Z}}_N \cdot \underline{\underline{A}}_N \cdot \underline{\underline{\Lambda}}_N^{-1} \equiv \underline{\underline{S}}_N \cdot \underline{\underline{\Lambda}}_N^{-1}$. The $P \times N$ score matrix is then

$$\underline{\underline{S}}_N = \underline{\underline{U}}_N \cdot \underline{\underline{\Lambda}}_N. \tag{23}$$

Hence, the SVD of the stir data in $\underline{\underline{Z}}$ enables the ACM to be decomposed into PC dyadics as

$$\underline{\underline{K}}_N = \left\langle \underline{\underline{A}}_N \cdot \underline{\underline{\Lambda}}_N^2 \cdot \underline{\underline{A}}_N^T \right\rangle = \sum_{n=1}^{N} \lambda_n^2 \underline{a}_n \underline{a}_n^T. \tag{24}$$

Physically, each successive (nth) PC adds a "layer" of stir energy in $\underline{\underline{K}}_N$. The $\det(\underline{\underline{K}}_N)$ is then a metric for the generalized variance of the energy stirred by N PCs, which is maximized by the PCA as well.

D. Residual Error for Reconstructed Data

From (2), (22), and (23), it follows that the original data matrix can be approximated from its truncated scores as

$$\underline{\underline{Z}}_N = \underline{\underline{S}}_N \cdot \underline{\underline{A}}_N^T. \tag{25}$$

The representation by less than M variables introduces an approximation error $\|\underline{\underline{Z}} - \underline{\underline{Z}}_N\|$, where $\|\cdot\|$ is a suitably chosen norm. From (2), i.e., $\underline{\underline{S}}_N = \underline{\underline{Z}} \cdot \underline{\underline{A}}_N$, combined with (25), it follows that

$$\begin{aligned} \left\| \underline{\underline{Z}} - \underline{\underline{Z}}_N \right\|^2 &= \left\| \underline{\underline{Z}} \cdot \left(\underline{\underline{I}} - \underline{\underline{A}}_N \cdot \underline{\underline{A}}_N^T \right) \right\|^2 \\ &\le \left\| \underline{\underline{Z}} \right\|^2 \left\| \underline{\underline{I}} - \underline{\underline{A}}_N \cdot \underline{\underline{A}}_N^T \right\|^2. \end{aligned} \tag{26}$$

V. PCA Interpretation

A. Geometric Interpretation of Unrotated PCs

Geometrically, $\underline{\psi}_n$ defines the direction of maximum spread of data in the remainder $(M - n + 1)$-dimensional (sub)space that is also mutually orthogonal to all $n - 1$ previous $\underline{\psi}_{n'}$ $(n' = 1, \ldots, n-1)$. PCA transforms the original correlated stir sequences into N new orthogonal functions ("axes"), i.e., PCs with associated uncorrelated coefficients ("coordinates," i.e., scores for the specific observations). In Section VI, the PCs are interpreted in terms of stir quantities.

The PCs can also be interpreted in terms of the Euclidean distance [12]: transforming the M stir states to a subset of N linear combinations corresponds to projecting the P vectors in M-dimensional space onto a subspace of dimension $N \le M$. The Euclidean distances between all pairs of stir sequences within this subspace are their projected lengths, whose sum of squares is then maximized (i.e., maximum accounted stirred energy) if the subspace is defined as the span of the N largest PCs, while minimizing the distance of each stir sequence to this subspace (minimum unaccounted stirred energy), to provide a hyperplane of best fit.

B. Rotation of PCs and Their Physical Interpretation

Rotational transformation of the extracted PCs often facilitates their physical interpretation (here, with reference to the original stir states and stir parameters), in spite of the fact that

it eliminates the hierarchy between PCs [32]. Oblique rotations [33] allow for larger separation between rotated PCs, resulting in PC loadings that are closer to ± 1 or 0 than for orthogonal rotations, and are hence more easily interpretable. However, losing orthogonality between PC axes as a result of maximizing this separation is undesirable in MT/MSRC stir optimization. Given a choice, in the present application it is more important to preserve the orthogonality of the loading vectors in rotated PCs than the uncorrelatedness of their scores because, for centered $\underline{Y}$ or $\underline{Z}$, this orthogonality defines the decorrelation between the stir components, while the scores relate to correlation between their associated amplitudes for the transformed field.

Orthogonal rotation (e.g., varimax [27]) preserves orthogonality of PCs, provided it is used with standard normalization $\underline{\underline{A}}_N^T \cdot \underline{\underline{A}}_N = 1$. To show this, consider the rotated loading matrix is $\underline{\underline{A}}'_N = \underline{\underline{A}}_N \cdot \underline{\underline{R}}_N$, where the prime denotes rotation with its associated transformation matrix $\underline{\underline{R}}_N$ being orthogonal, i.e., $\underline{\underline{R}}_N^T \cdot \underline{\underline{R}}_N = \underline{\underline{I}}$. Hence,

$$\underline{\underline{A}'}_N^T \cdot \underline{\underline{A}}'_N = \underline{\underline{R}}_N^T \cdot \left(\underline{\underline{A}}_N^T \cdot \underline{\underline{A}}_N\right) \cdot \underline{\underline{R}}_N = \underline{\underline{I}} \tag{27}$$

i.e., orthonormality of PCs after rotation is preserved. For the rotated score matrix $\underline{\underline{S}}'_N$, however, substituting $\underline{\underline{S}}_N = \underline{\underline{Z}}_N \cdot \underline{\underline{A}}_N$ and $\underline{\underline{A}}_N^T \cdot \underline{\underline{A}}_N = \underline{\underline{I}}$ with the SVD (22) yields

$$\underline{\underline{S}'}_N^T \cdot \underline{\underline{S}}'_N = \underline{\underline{R}}_N^T \cdot \left(\underline{\underline{A}}_N^T \cdot \underline{\underline{A}}_N\right) \cdot \left(\underline{\underline{\Lambda}}_N \cdot \underline{\underline{U}}^T \cdot \underline{\underline{U}} \cdot \underline{\underline{\Lambda}}_N\right) \cdot \left(\underline{\underline{A}}_N^T \cdot \underline{\underline{A}}_N\right) \cdot \underline{\underline{R}}_N = \underline{\underline{R}}_N^T \cdot \underline{\underline{\Lambda}}_N^2 \cdot \underline{\underline{R}}_N \neq \underline{\underline{\Lambda}}_N^2. \tag{28}$$

Since $\underline{\underline{R}}_N^T \cdot \underline{\underline{\Lambda}}_N^2 \cdot \underline{\underline{R}}_N$ is not diagonal, the rotated PC scores may now be correlated. With different normalizations of $\underline{a}_n$, one can arrange for either the rotated scores to remain mutually uncorrelated or for the rotated loading vectors to remain mutually orthogonal, but never both simultaneously and possibly neither [34].

Since stirring is a process of continuous variation of the field, rotated PCs can be expected to form clusters of *adjacent* stir states. Hence, for mechanical rotational stirring, the PCs represent fields stirred by *angular sectors* of the paddle wheel. Thus, the outcome of PCA is a set of (central) angular locations and opening angles of circle sectors ranked from high to low according to their stir performance. This will be further demonstrated in Section VI-F.

C. Decentralization and Unstandardization

The PCs, loadings and scores for $\underline{\underline{Z}}_N$ can be transformed back to those for the original decentered and unstandardized field data $\underline{\underline{X}}_N$, enabling their absolute contributions to the overall stir performance to be intercompared. With $\underline{\underline{K}}_{Z_N} = \langle \underline{Z}_n \, \underline{Z}_n^T \rangle = \lim_{P\to\infty} \overline{\underline{\underline{Z}}_N^T \cdot \underline{\underline{Z}}_N}/P$ for $\underline{\underline{Z}}_N = [\underline{Z}_n]_{n=1}^N \triangleq [(\underline{X}_n - \langle \underline{X}_n \rangle)/\sigma_{\underline{X}_n}]_{n=1}^N$ and $\underline{\underline{C}}_{X_N} = \langle \underline{X}_n \, \underline{X}_n^T \rangle - \langle \underline{X}_n \rangle \langle \underline{X}_n \rangle^T = \lim_{P\to\infty} [\overline{\underline{\underline{X}}_N^T \cdot \underline{\underline{X}}_N} - (\overline{\underline{X}_N} \, \underline{1}^T) \cdot (\underline{1} \, \overline{\underline{X}_N}^T)]/P$ for $\underline{\underline{X}}_N = [\underline{X}_n]_{n=1}^N$ with $\underline{1} \triangleq [1]_{p=1}^P$, substitution yields

$$\underline{\underline{C}}_{X_N} = \underline{\underline{\Sigma}}_{X_N} \cdot \underline{\underline{K}}_{Z_N} \cdot \underline{\underline{\Sigma}}_{X_N} \tag{29}$$

where $\underline{\underline{\Sigma}}_{X_N} \triangleq \mathrm{diag}(\sigma_{\underline{X}_1}, \ldots, \sigma_{\underline{X}_N})$. Since $\underline{\underline{A}}_{X_N}$ and $\underline{\underline{A}}_{Z_N}$ are invertible, the eigendecompositions $\underline{\underline{K}}_{Z_N} = \underline{\underline{A}}_{Z_N} \cdot \underline{\underline{\Lambda}}_{Z_N}^2 \cdot \underline{\underline{A}}_{Z_N}^{-1}$ and $\underline{\underline{C}}_{X_N} = \underline{\underline{A}}_{X_N} \cdot \underline{\underline{\Lambda}}_{X_N}^2 \cdot \underline{\underline{A}}_{X_N}^{-1}$ lead to the EVE identity

$$\underline{\underline{A}}_{X_N} \cdot \underline{\underline{\Lambda}}_{X_N}^2 \cdot \underline{\underline{A}}_{X_N}^{-1} = \underline{\underline{\Sigma}}_{X_N} \cdot \underline{\underline{A}}_{Z_N} \cdot \underline{\underline{\Lambda}}_{Z_N}^2 \cdot \underline{\underline{A}}_{Z_N}^{-1} \cdot \underline{\underline{\Sigma}}_{X_N} \tag{30}$$

whose solution $\underline{\underline{A}}_{X_N}$ yields the PCs of $\underline{\underline{X}}$ as a function of those of $\underline{\underline{Z}}$. If the PC directions and loadings are maintained upon unstandardization, then the EVAs remain unchanged as well. More generally, however, the EVA matrices are merely similar, i.e.,

$$\underline{\underline{\Lambda}}_{X_N}^2 = \left(\underline{\underline{A}}_{X_N}^{-1} \cdot \underline{\underline{\Sigma}}_{X_N} \cdot \underline{\underline{A}}_{Z_N}\right) \cdot \underline{\underline{\Lambda}}_{Z_N}^2 \cdot \left(\underline{\underline{A}}_{X_N}^{-1} \cdot \underline{\underline{\Sigma}}_{X_N} \cdot \underline{\underline{A}}_{Z_N}\right)^{-1}. \tag{31}$$

The scores $\underline{\underline{S}}_{Z_N} = \underline{\underline{Z}}_N \cdot \underline{\underline{A}}_{Z_N}$ for $\underline{\underline{Z}}_N = (\underline{\underline{X}}_N - \underline{1} \, \overline{\underline{X}_N}^T) \cdot \underline{\underline{\Sigma}}_{X_N}^{-1}$ are unstandardized as $\underline{\underline{S}}_{X_N} = \underline{\underline{X}}_N \cdot \underline{\underline{A}}_{X_N}$ in accordance with

$$\underline{\underline{S}}_{X_N} = \left(\underline{\underline{S}}_{Z_N} \cdot \underline{\underline{A}}_{Z_N}^{-1} \cdot \underline{\underline{\Sigma}}_{X_N} + \underline{1} \, \overline{\underline{X}_N}^T\right) \cdot \underline{\underline{A}}_{X_N}. \tag{32}$$

VI. Experimental Results

As noted in Section III-D, for a fixed measurement frequency, choosing spatial location as the observation parameter would constitute an optimal choice for investigating the LUF in several respects. However, collecting high-definition data in the stir-space domain is considerably more time consuming than in the stir-frequency domain and was not feasible with the available instrumentation. Our stir-frequency domain measurements, i.e., with frequency as observation parameter at a fixed single location of the sensor and stir state as the variable, serve as a valid yet suboptimal dataset for demonstrating PCA for the selection of optimum stir states.

In order to separate nonstationarity in the stir domain from that in the time domain, data obtained using mode-tuned (as opposed to mode-stirred) operation are examined. Specifically, we analyze data for the function

$$X(f,m) \triangleq \mathrm{Re}\left[\frac{S_{21}(f,m)}{[1-S_{11}(f,m)][1-S_{22}(f,m)]}\right] \tag{33}$$

measured inside a MTRC using two biconical antennas, at $M = 1000$ equal tuner positions ($\Delta\tau = 0.36°$), with $\tau_m \equiv m\Delta\tau$. First, values of $X(\cdot, m)$ were measured between 50 and 148 MHz in equal frequency steps of 2 MHz. After experimenting with a few different frequency steps, this value was justified by inspection of the frequency ACM[3], indicating that $|\rho_X(f_k, f_\ell)| < 0.3, \ldots, 0.4$ at nearly all frequency pairs, i.e., $P \simeq 50$. A frequency step smaller than 2 MHz increased the effective value of P only marginally, because of increased correlation between frequencies. Results were calculated for both covariance- and correlation-based PCA, but were found to be almost indistinguishable. The reported results here are for covariance-based PCA, because of its greater pertinence when

[3]Not shown here due to space limitations, but of similar appearance as Fig. 8 although somewhat less uniform, and with frequency instead of stir state as its axes. Generally, correlation between observations does not affect the validity of PCA for descriptive analysis [15].

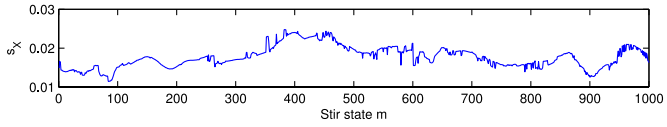

Fig. 1. Standard deviation s_{X_m} within frequency responses across the 50–148 MHz band, as a function of stir state m.

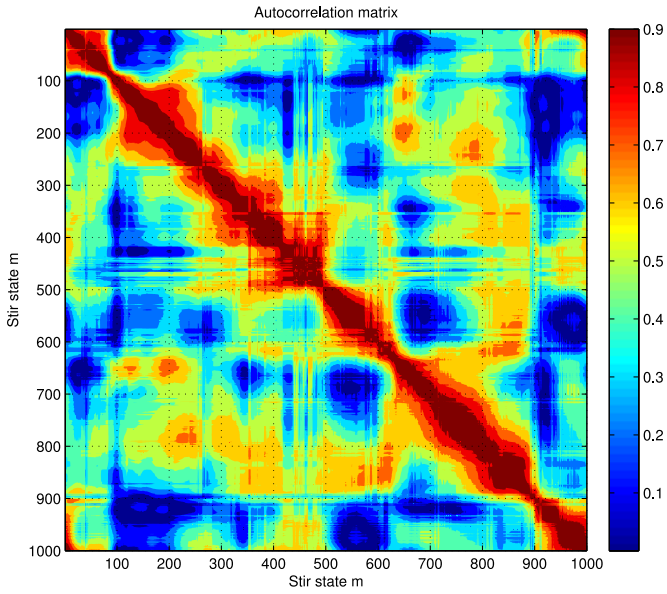

Fig. 2. Correlation matrix (magnitude) of 1000 stir states across the 50–148 MHz band.

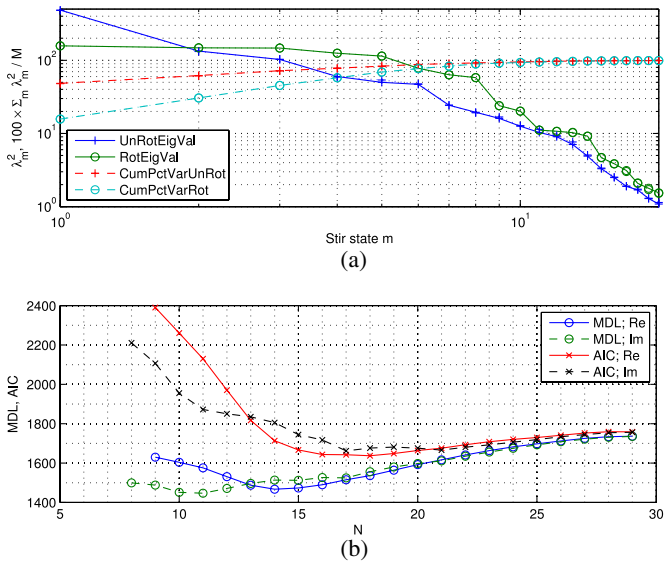

Fig. 3. (a) Unrotated and varimax rotated eigenvalues of extracted PCs ($\lambda_m^2 > 1, N = 20$) and their cumulative percentage of stirred energy contribution across the 50–148 MHz band. (b) MDL(N) and AIC(N) for real and imaginary parts of normalized $S_{21}(f, m)$.

all PCA variables have a similar scale of variation and the same physical unit.

A. Standard Deviation

Fig. 1 shows that the sample standard deviation $s_X(m)$ of the frequency responses changes by less than a factor 2.3 across the stir states, but with no clear trend. The stir states $350 < m < 450$ are earmarked as potentially more efficient, based on their higher values of $s_X(m)$. However, without additional knowledge of their mutual correlation, their fluctuations could range in their level of similarity.

B. Autocorrelation Matrix

Fig. 2 shows the symmetric $M \times M$ ACM. The extensive departures from an ideal Töplitz structure (i.e., color bands that are ideally parallel to its main diagonal) indicate that this stirring process is significantly non-WSS. For an arbitrary variance, stir states with strongly dissimilar stir sequences are more likely to accumulate to a larger total stirred energy. The primary interest is therefore in finding clusters of weakly correlated stir states, shown as "deep blue pools" in the ACM, e.g. near (120,30) and (670, 40). "Large red plains" indicate strongly correlated states with similar stir performances that are *individually* potentially good, e.g., near (160,160), (700,700), and (400,400), where red/orange areas are relatively wide. Horizontal or vertical strips in the matrix that combine both features show the clearest contrast between state correlations, e.g., the bands $100 < m < 250$, $500 < m < 600$, $650 < m < 750$, $900 < m < 1000$, but not e.g. $350 < m < 450$, which has only a small blue area, despite a wider red area around the main diagonal. Combined with Fig. 1, this suggest that while the latter sector might provide adequate stirring, it is likely to form a region of correlation (overlap, if adjacent) between two or more other good stir sectors and is hence poorly accumulating. By contrast, the pair of states $m_1 = 970$ and $m_2 = 570$ combine well because they are strongly uncorrelated (see Fig. 2) *and* exhibit relatively high values of $s_X(m_1)$ and $s_X(m_2)$ (see Fig. 1).

C. Eigenvalues

Fig. 3 shows the first $N = 20$ ranked EVAs λ_n^2 as extracted on the basis of the Guttman–Kaiser criterion ($\lambda_m^2 > 1$). Varimax rotation of the extracted PCs is seen to produce a more uniform spread of EVAs: for example, the first and tenth EVAs represent the energy equivalent of 484.5 and 12.5 average stir states before rotation, compared to 157.6 and 20.2 afterward, respectively. The shown cumulative EVA percentage $(100 \times \sum_m \lambda_m^2/M)\%$ measures the relative amount of stirred energy accounted for by the first m PCs. Unrotated EVAs are seen to outperform rotated EVAs on this basis because of the much larger first EVA value. Thus, while the total extracted stirred energy maximized by PCA remains unchanged after rotation, its distribution across the PCs becomes more equalized by rotation, with much reduced hierarchy between them.

We also estimated N from the AIC and MDL criteria (10), for the real and corresponding imaginary part of the bracketed expression in (33). Compared to the Guttman–Kaiser value, the

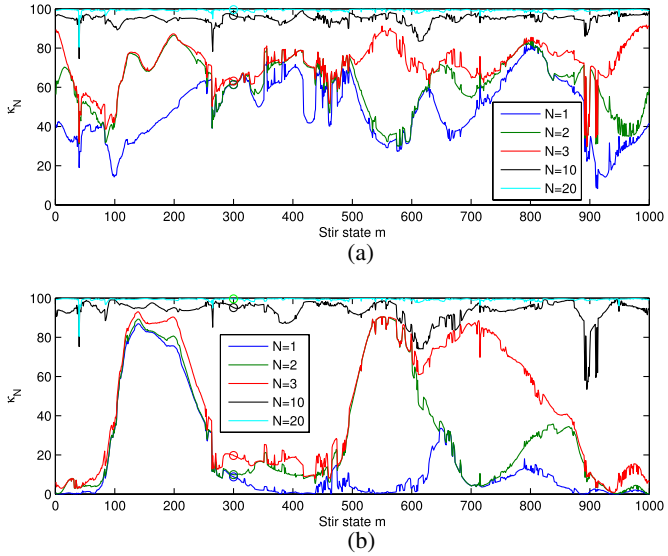

Fig. 4. Communalities of N extracted PCs, as a percentage of the total stirred energy produced by stir state m, across the 50–148 MHz band: (a) unrotated and (b) varimax rotated PCs.

MDL and AIC estimates are somewhat more conservative (minima reached at $N = 14$ and 18 for (33), respectively). These estimates were found to increase rather sensitively when increasing M.

D. Communalities

A detailed breakdown of the fraction of stirred energy by N PCs across individual stir states m is given by the cumulative communalities, shown in Fig. 4(a). Each set of unrotated PCs focuses on variation across different regions of m, e.g., the first unrotated PC primarily accounts for energy around $m \simeq 800$. Nevertheless, the PCs contain substantial contributions from all stir states. The performance of some isolated stir states is less than average throughout. For example, at $m = 41$ the 20 extracted PCs account for much less stirred energy than for any other m, with the remainder 980 residual components still accounting for 19.5 % of the energy stirred by the 41st state.

For the rotated PCs, Fig. 4(b) indicates that the contribution of each rotated PC is now more concentrated around particular stir states. For example, most stir states within $100 < m < 250$ are prominent in the first rotated PC, although they make a less than average contribution to the first unrotated PC.

E. Standardized Rotated PCs: Loadings and Interpretation

Grouping the contributions of individual stir states to rotated PCs yields their ranked loadings. Their squared values are shown in Fig. 5(a) (top). For clarity, only the first 12 PCs are shown, although rotation was performed on all 20 extracted PCs. After unranking, the groups of stir states that constitute each PC form clusters of values of m [see Fig. 5(a) (bottom)]. A physical interpretation of the rotated PCs thus follows as being associated with the energy stirred by specific *angular sectors* of correlated stir states. These sectors are in general not symmetric around their peak loadings, nor do the clusters have equal width or equally spaced centers. This demonstrates again that stirring performance is not uniform across one revolution.

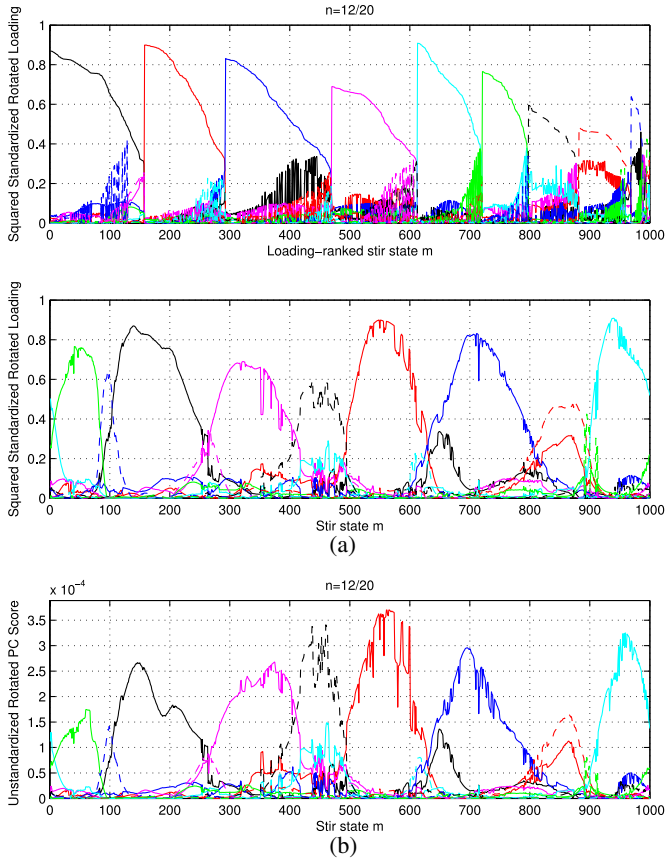

Fig. 5. First 12 of 20 varimax rotated PCs across the 50–148 MHz band: (a) ranked (top) and unranked (bottom) standardized PC loadings, and (b) unstandardized unranked PC scores.

F. Unstandardized Rotated Loadings

Rotated loadings identify sets of angular sectors, but do not permit for their stir performance to be intercompared because rotation may remove the hierarchy among the EVAs of the rotated PCs. To restore ranking, the scores for the unstandardized data can be calculated from (32), which involves accounting for the standard deviations $s_X(m)$ shown in Fig. 1.

As an application, the IEC 61000-4-21 specification for MT/MSRC validation and testing stipulates a minimum of 12 stir states [9, Table B.1] . Particularly, near the LUF, identification of the optimum 12 stir states can be critically important with regard to pass/fail, yet using trial-and-error based on equiangular stir steps can be time consuming and suboptimal. Moreover, if the 12 PC sectors are not equiangular nor uniformly spaced (non-WSS stir process), then one or more of them can be easily missed when using equiangular stepping. The identification of the angular positions in the smallest possible set of *combined* stir states that meet this limit offers greater economy. Selecting the stir states at the crests of each of the 12 unstandardized PCs represents an optimum selection: Fig. 5(b) shows that the ordered set of optimum stir states for maximum energy stirring in the 50–148 MHz interval is then:

566, 460, 959, 696, 375, 146, 60, etc.

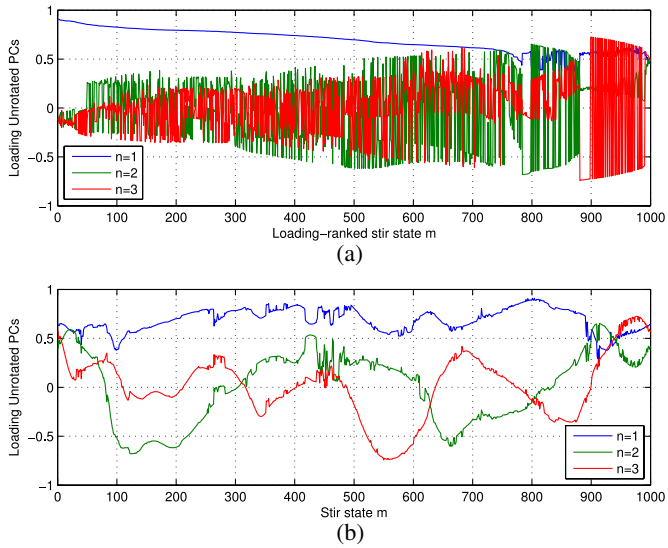

Fig. 6. First three unrotated PCs across the 50–148 MHz band: (a) as a function of ranked stir states, ordered by their unweighted contribution to stirred field, (b) as a function of actual stir states.

Compared to the standardized loadings, the width and shape of the profiles are not much affected. However, the relative heights have changed, particularly near the maxima. For $N > 12$, the optimum set may have one or more of these 12 PCs substituted by other ones. As noted in Section III-D, other frequency intervals may lead to different PCs and, hence, different sectors of stir angles when using frequency as observation variable. For optimization at a single frequency, observation data based on spatial scanning of the receiving antenna are recommended.

G. Unrotated PCs

With the insight provided by rotated PCs, one may attempt to interpret the unrotated PCs as well. The first three of these are shown in Fig. 6. Unlike rotated PCs for standardized data, they exhibit a hierarchy. As seen from Fig. 6(a), the first, second and third PC dominate across sectors of 784, 97 (=881−784) and 119 (=1000−881) stir states, respectively, but with rapidly decreasing magnitude. While some complementary features occur in Fig. 6(b) (e.g., notches between the 418th to 439th state in PCs 1 (blue) and 2 (green)), each PC makes substantial contributions to all 1000 stir states. The first PC has strictly positive loadings, suggesting that it represents the average "dc" contribution of stirred energy across all stir states. Combined with the bipolar second and third PC, the features of $s_X(m)$ in Fig. 1 gradually emerge on steadily smaller scales of m (cf., its evolution near $m \simeq 100$ and for $850 < m < 1000$, respectively).

H. High-Frequency PCs

For comparison, we present the main results for a band of higher frequencies in the overmoded regime, between 900 and 998 MHz. Here, the Guttman–Kaiser criterion extracted $N = 49$ PCs.[4] The standard deviations, ACM, EVAs, the first 12 standardized and unstandardized rotated PC loadings, and the first three unrotated PCs are shown in Figs. 7–11. On average, $s_X(m)$ is now more uniform (see Fig. 7). The extracted EVAs have a smaller dynamic range before rotation, while being still more uniformly spread after rotation (see Fig. 9). Comparison of Figs. 8 and 10 indicates that stir sectors near $m \simeq 250, \ldots, 280, 450$, and 700 are marginally larger than others, while a horizontal band of small correlations near $m \simeq 950, \ldots, 1000$ is accompanied by lower $s_X(m)$. The generally small correlations away from the main diagonal and the greater homogeneity of $s_X(m)$ indicate that all 49 selected stir states for 900–998 MHz are now more uniformly distributed and less overlapping than for the 50–148 MHz band. However, the differences between the scores of the rotated unstandardized PCs [see Fig. 10(b)] are still not negligible, indicating that variation in the average stirred energy remains, even at these relatively high frequencies. The unrotated

[4]Since now $P = 50 \not\gg N$ when $\Delta f = 2$ MHz, the accuracy of the calculated EVEs and hence PCs is more limited.

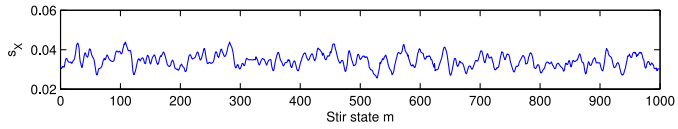

Fig. 7. Standard deviation s_{X_m} within frequency responses across the 900–998 MHz band as a function of stir state.

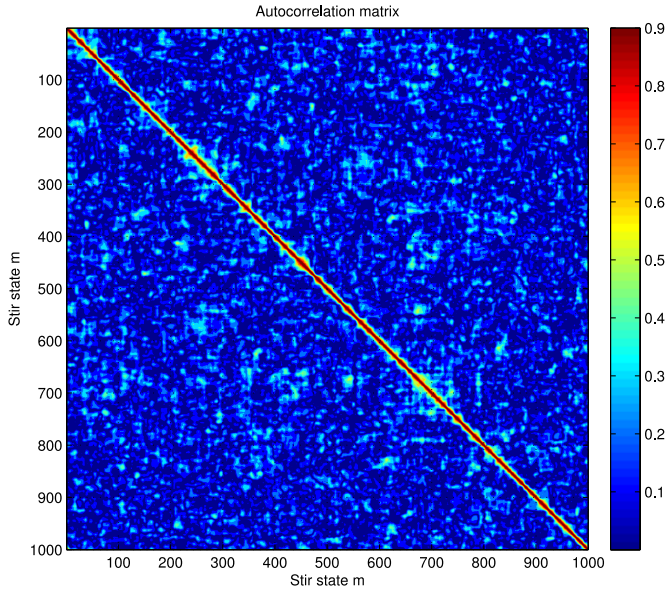

Fig. 8. Correlation matrix (magnitude) of 1000 stir states across the 900–998 MHz band.

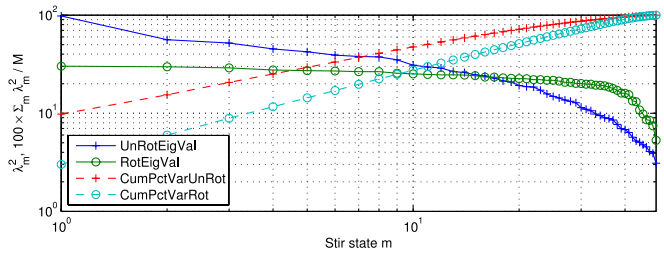

Fig. 9. Unrotated and varimax rotated eigenvalues of extracted PCs ($\lambda_m^2 > 1$) and their cumulative percentage of stirred energy contribution across the 900–998 MHz band.

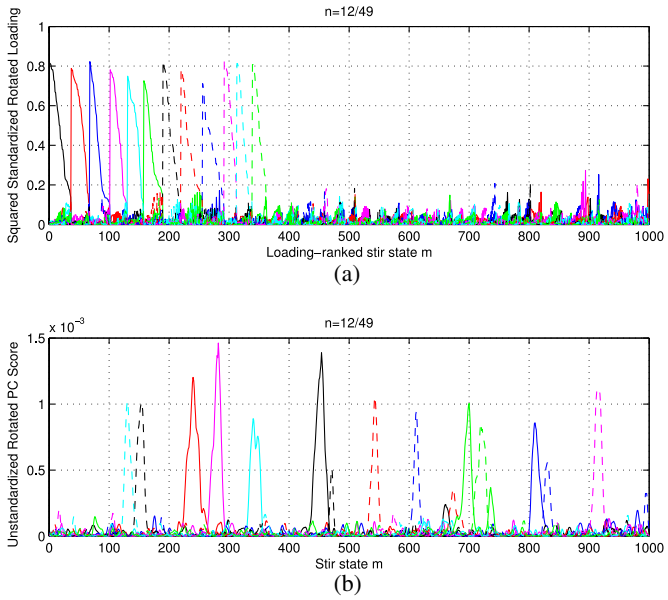

Fig. 10. First 12 of 49 varimax rotated PCs across the 900–998 MHz band: (a) ranked standardized PC loadings, (b) unstandardized PC scores.

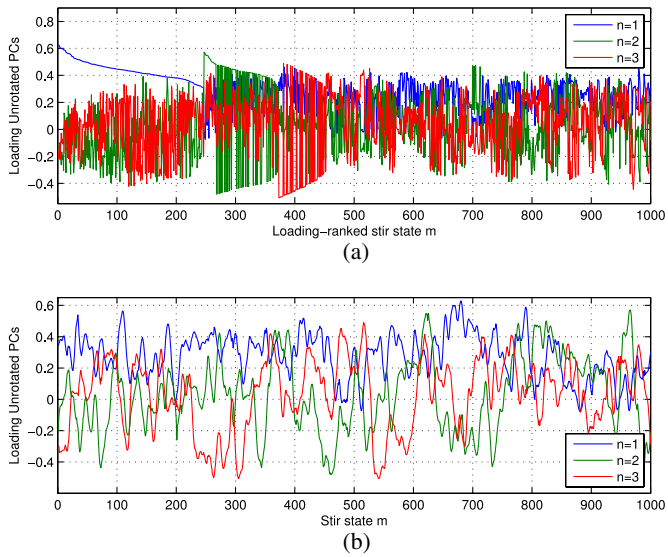

Fig. 11. First three unrotated PCs across the 900–998 MHz band: (a) as a function of ranked stir states, ordered by their unweighted contribution to stirred field, (b) as a function of actual stir states.

PCs (see Fig. 11) have now more similar average loadings and are more evenly spread, with the first PC now dominating over fewer than a third of the stir states in the 50–148 MHz range, without dominance of any of the first three PC across more than half of the stir states.

VII. Dual PCA: Principal Frequencies

PCA can also be used in a converse manner, viz., by assigning the P frequency components of the field to be the variables (data columns), with the stir states at an arbitrary frequency now serving as observation samples (rows) $\underline{Z}_m^T$, where sample averaging is now across all M stir states. The goal is then, on the basis of M chamber responses at different stir states, per frequency, to extract N out of P dominant frequency components ("signals") from the spectrum of the MT/MSRC as being principal frequency components. Since these PCs are associated with frequencies yielding the largest share of the variance of the field, they represent the part of the spectrum that is most volatile under mechanical stirring action. From a different perspective, these frequencies produce maximally efficient electronic stirring. These extracted principal frequencies or subbands can also be used to compile a list of efficient (possibly irregularly spaced) test frequencies within a specified interval [2], [9]. If data over a wide band need to be analyzed, then one must take into account that the fraction of stirred energy is usually smaller at lower frequencies than at higher ones (heteroscedasticity). Hence, in this case, covariance based-PCA is not applicable for principal frequency extraction, and correlation-based PCA is necessary to compensate for the disproportionally large weight of high-frequency components.

Principal frequencies are easily extracted from the SVD (22) by noting that the columns of $\underline{\underline{U}}$ are the EVEs for the new ACM $\underline{\underline{K}}^T = \langle \underline{Z}^T \, \underline{Z} \rangle \simeq \overline{\underline{z} \cdot \underline{z}^T}/M$, as opposed to taking the columns of $\underline{\underline{A}}$ as EVEs of $\underline{\underline{K}} = \langle \underline{Z} \, \underline{Z}^T \rangle \simeq \overline{\underline{z}^T \cdot \underline{z}}/P$ earlier.

VIII. PCs as Eigenstirrings

The analysis of the measured data permits the following interpretation. A stir sequence of sampled field values across M stir states represents a unique point in an M-dimensional stir space for each one of P measured frequencies. Generally, EVEs are interpretable in PCA as *modes* of variation in the data, while the EVAs are their associated modal amplitudes [14]. In the context of MT/MSRCs, all M EVEs associated with the OE or PCs of $\underline{\underline{Z}}$ can thus be designated as *eigenstirrings* or *stir modes*,[5] forming empirical eigenmodes in the stir domain. For example, the first three eigenstirrings in the 50–148 MHz band are shown in Fig. 6(b), after normalizing by their integrated squared value. Since the EVEs are orthonormal, they form a set of basis functions for expanding any individual stir sequence across the specified frequency range. The interpretation of stir modes is thus similar to cavity modes that form eigenmodes in the spatial domain: just like cavity modes represent normalized patterns of spatial variation of amplitude at locations $\mathrm{P}(x, y, z)$ as produced by superpositions of travelling waves, stir modes are patterns of fundamental fluctuations of the stirred field across the stirrer that combine to the total extracted stirred energy at stir state τ_m.

While a full set of M stir modes allows for exact expansion and representation of the stir sequence, correlations between the M sequences makes the set partially redundant and allows for reducing it to a smaller set of N stir modes with almost equal total stirred energy.

In the limit $N \to \infty$, stir modes become asymptotically equivalent to individual stir states (stir angles, i.e., zero-width stir sectors), because then any incremental change in stir state gives rise to a nonneglible contribution to the stirred energy. In this case, the ACM $\underline{\underline{K}}$ has Töplitz structure and the eigenfunctions $\underline{\psi}_n(\tau)$ are trigonometric [17], [35].

[5]Not to be confused with 'stirred modes', referring to dynamic spatial modes.

IX. Conclusion

In this paper, PCA was applied to characterize nonstationarity in the stir domain. Rotated PCs can be interpreted as energy stirred by specific angular sectors of a rotating mode stirrer. Close agreement was found between properties of extracted PCs and features found in the ACM combined with the variation of the standard deviation across stir sequences.

Presuming that stir states are WSS, thus considering them as statistically equivalent, ignores possible differences in their stir efficiency. This can potentially lead to suboptimal stirring, particularly at lower frequencies. The ability to rank stir states assists in selecting the best subset and helps to improve understanding about the effect of geometric design and operational features on stir quality. In the frequency domain, this is a familiar situation: at any given stir position in an undermoded MT/MSRC, a spectrum analyzer can detect spectral islands of above-average density of cavity eigenmodes that offer better scope for more efficient stirring than sparse frequency bands. In analogy, OE and PCA provide a *stir analyzer* for detecting stir states with above-average stir efficiency within a given spectral band. In the highly overmoded regime, nonstationarity in the stir domain may become negligibly small, whence ranking stir states may be less advantageous. While we concentrated on PCA as a statistical data analysis tool, probabilistic PCA theory can be applied to build inferential models, in particular PDFs of PCs for Gaussian data [36].

While the focus of this paper is on MT/MSRCs, PCA is a versatile technique that is likely to benefit other areas of EMC and other applications of stochastic electromagnetism as well.

References

[1] P. Corona, G. Ferrara, and M. Migliaccio, "Reverberating chambers as sources of stochastic electromagnetic fields," *IEEE Trans. Electromagn. Compat.*, vol. 38, no. 3, pp. 348–356, Aug. 1996.

[2] L. R. Arnaut, "Maximum rate of frequency scanning for distortionless signal generation in electromagnetic reverberation chambers," *IEEE Trans. Electromagn. Compat.*, vol. 50, no. 4, pp. 787–793, Nov. 2008.

[3] L. R. Arnaut, "On the maximum rate of fluctuation in mode-stirred reverberation," *IEEE Trans. Electromagn. Compat.*, vol. 47, no. 4, pp. 781–804, Nov. 2005.

[4] J. M. Dunn, "Local, high-frequency analysis of the fields in a mode-stirred chamber," *IEEE Trans. Electromagn. Compat.*, vol. 32, no. 1, pp. 53–58, Feb. 1990.

[5] A. Somani, S. Gorla, M. Magdowski, and R. Vick, "Measurement of boundary fields in a reverberation chamber," in *Proc. 10th Eur. Symp. Electromagn. Compat.*, York, U.K., Sep. 2011, pp. 26–30.

[6] L. R. Arnaut and D. A. Knight, "Observation of coherent precursors in pulsed mode-stirred reverberation fields," *Phys. Rev. Lett.*, vol. 98, pp. 053903-1–053903-4, Feb. 2007.

[7] L. R. Arnaut, "Statistical characterisation of dynamic propagation environments for mobile wireless communication systems," in *Proc. 19th IMEKO World Congr. Metrol.*, Lisbon, Portugal, 2009, pp. 2315–2318.

[8] L. R. Arnaut, "Time-domain measurement and analysis of mechanical step transitions in mode-tuned reverberation: Characterization of instantaneous field," *IEEE Trans. Electromagn. Compat.*, vol. 49, no. 4, pp. 772–784, Nov. 2007.

[9] *IEC 61000-4-21 Electromagnetic Compatibility (EMC): Part 4: Testing and Measurement Techniques: Section IV: Reverberation Chambers*, 2nd ed., IEC, Geneva, Switzerland, Jan. 2011.

[10] O. Lundén and M. Bäckström, "Stirrer efficiency in FOA reverberation chambers. evaluation of correlation coefficients and chi-squared tests," in *Proc. IEEE Int. Symp. Electromagn. Compat.*, Washington, DC, USA, Aug. 2000, pp. 11–16.

[11] F. Moglie and V. M. Primiani, "Analysis of independent positions of reverberation chamber stirrers as a function of their operating conditions," *IEEE Trans. Electromagn. Compat.*, vol. 53, no. 2, pp. 288–295, May 2011.

[12] K. Pearson, "On lines and planes of closest fit to systems of points in space," *Phil. Mag.*, vol. 6, no. 2, pp. 559–572, 1901.

[13] H. Hotelling, "Analysis of a complex of statistical variables into principal components," *J. Edu. Psychol.*, vol. 24, pp. 417–441, 1933.

[14] R. W. Preisendorfer, *Principal Component Analysis in Meteorology and Oceanography*. Amsterdam, the Netherlands: Elsevier, 1988.

[15] I. T. Jolliffe, *Principal Component Analysis*, 2nd ed. New York, NY, USA: Springer-Verlag, 2002.

[16] L. R. Arnaut, "Spatial correlation functions of inhomogeneous random electromagnetic fields," *Phys. Rev. E*, vol. 73, no. 3, 036604-1–036604-11, Mar. 2006.

[17] L. R. Arnaut and P. D. West. (1998, Aug.). Evaluation of the NPL untuned reverberation chamber using mechanical and electronic stirring techniques. *NPL Report CEM 11*, ISSN 1369–6742, [Online]. Available: http://www.npl.co.uk/publications/

[18] L. R. Arnaut, "Uncertainty reduction and decorrelation of mode-stirred reverberation chamber data using transformation and expansion techniques," in *Proc. 4th Eur. Symp. Electromagn. Compat.*, Brugge, Belgium, Sep. 2000, pp. 213–218.

[19] L. R. Arnaut, "Untuned 3-D stadium reverberation chamber for microwave and millimeter-wave frequencies," in *Proc. Mode-Stirred Chamber Anechoic Chamber OATS Users Meeting*, Northbrook, IL, USA, Jun. 1999, pp. 1–6.

[20] H. G. Krauthäuser, T. Winzerling, J. Nitsch, N. Eulig, and A. Enders, "Statistical interpretation of autocorrelation coefficients for fields in mode-stirred chambers," in *Proc. IEEE Int. Symp. Electromagn. Compat.*, Chicago, IL, USA, Aug. 2005, pp. 550–555.

[21] C. Lemoine, P. Besnier, and M. Drissi, "Advanced method for estimating number of independent samples available with stirrer in reverberation chamber," *Electron. Lett.*, vol. 43, no. 16, pp. 861–862, Aug. 2007.

[22] C. Lemoine, P. Besnier, and M. Drissi, "Estimating the effective sample size to select independent measurements in a reverberation chamber," *IEEE Trans. Electromagn. Compat.*, vol. 50, no. 2, pp. 227–236, May 2008.

[23] R. J. Pirkl, K. A. Remley, and C. S. Lötbäck Patané, "Reverberation chamber measurement correlation," *IEEE Trans. Electromagn. Compat.*, vol. 54, no. 3, pp. 533–545, Jun. 2012.

[24] H. G. Krauthäuser, "Number of samples required to meet a field inhomogeneity limit with given confidence in reverberation chambers," *IEEE Trans. Electromagn. Compat.*, vol. 54, no. 5, pp. 968–975, Oct. 2012.

[25] A. Marín-Soler, M. Grudén, J. D. Sánchez-Heredia, P. Hallbjörner, A. M. Martínez-González, A. Rydberg, and D. A. Sánchez-Hernández, "Sample selection algorithms for enhanced MIMO antenna measurements using mode-stirred reverberation chambers," *IEEE Trans. Antennas Propag.*, vol. 60, no. 8, pp. 3892–3900, Aug. 2012.

[26] P. R. Peres-Neto, D. A. Jackson, and K. M. Somers, "How many principal components? Stopping rules for determining the number of non-trivial axes revisited," *Comp. Stat. Data Anal.*, vol. 49, pp. 974–997, 2005.

[27] H. F. Kaiser, "The varimax criterion for analytic rotation in factor analysis," *Psychometrika*, vol. 23, no. 3, pp. 187–200, Jun. 1958.

[28] A. N. Kolmogorov, "Three approaches to the quantitative definition of information," *Probl. Inf. Transmiss.*, vol. 1, pp. 3–11, 1965.

[29] M. Wax and T. Kailath, "Detection of signals by information criteria," *IEEE Trans. Acoust. Speech Signal Process.*, vol. 33, no. 2, pp. 387–392, Apr. 1985.

[30] H. T. Eastment and W. J. Krzanowski, "Cross-validatory choice of the number of components from a principal component analysis," *Technometrics*, vol. 24, pp. 73–77, 1982.

[31] A. Bejan, *Largest Eigenvalues and Sample Covariance Matrices*. M.Sc. dissertation, Univ. Warwick, Coventry, U.K., Sep. 2005.

[32] M. B. Richman, "Rotation of principal components," *J. Climatatol.*, vol. 6, pp. 293–335, 1986.

[33] M. B. Richman, "Oblique rotation of principal components: An improved meteorological map typing technique?," *J. Appl. Meteor.*, vol. 20, pp. 1145–1159, Oct. 1981.

[34] I. T. Jolliffe, "Rotation of principal components: Choice of normalization constraints," *J. Appl. Stat.*, vol. 22, no. 1, pp. 29–35, 1995.

[35] D. R. Brillinger, *Time Series: Data Analysis and Theory*. San Francisco, CA, USA: Holden-Day, 1981.

[36] M. E. Tippet and C. M. Bishop, "Probabilistic principal component analysis," *J. R. Statist. Society, Ser. B*, vol. 61, no. 3, pp. 611–622, 1999.

Authors' photographs and biographies not available at the time of publication.